

Symmetric instability in the Atlantic Meridional Overturning Circulation

Fraser William Goldsworth

St Anne's College

University of Oxford

A thesis submitted for the degree of

Doctor of Philosophy

Trinity 2022



For Harriet

Acknowledgements

Some people to acknowledge

Abstract

Something abstract.

Contents

1	Introduction	1
1.1	The Atlantic Meridional Overturning Circulation	1
1.1.1	<i>The Western Boundary Current Systems of the Tropical Atlantic</i>	2
1.1.2	<i>The Irminger Current</i>	2
1.2	Potential vorticity & symmetric instability	2
1.2.1	<i>Ekman driven symmetric instability</i>	4
1.2.2	<i>Cross equatorial symmetric instability</i>	4
2	Symmetric instability	6
2.1	Inviscid symmetric instability of parallel shear flow	6
2.1.1	<i>The instability criterion</i>	8
2.1.2	<i>Orientation of the least stable modes</i>	9
2.1.3	<i>Gravitational & inertial instability as limiting cases of symmetric instability</i>	10
2.1.4	<i>Energetics of the instability</i>	11
2.1.5	<i>The classical and energetic definitions of symmetric instability</i>	12
2.2	Inviscid symmetric instability of axisymmetric flow	13
2.3	Viscous inertial instability	15
2.4	Viscous symmetric instability with the complete Coriolis force	20
3	Symmetric instability in a cross-equatorial surface current	26

4 Symmetric instability in a cross-equatorial deep western boundary current	27
4.1 Introduction	27
4.2 Methods	30
4.3 Results & discussion	32
4.4 A simplified model of staircse formation	34
4.5 Conclusions	37
5 Ekman driven symmetric instability in a high lattitude western boundary current	38

List of Figures

1.1 Caption	5
4.1 (a) A map of the tropical Atlantic and its bathymetry. Climatological profiles of neutral density were aggregated from the area enclosed by the red rectangle. Bathymetry data from ?. (b) Initial meridional velocity profile and density profile (solid line) used as initial conditions and boundary conditions for the model. The velocity profile is based on observations by Schott et al. (2005), and the density profile on the climatological mean (dashed line) (?).	31

4.2 Squared buoyancy frequency after 239 days of model integration plotted at (a) 250 km south of the equator, (b) 500 km south of the equator and (c) 600 km south of the equator. The figures show the presence of mixing barriers (thin filaments of strong stratification) separated by well mixed regions of low stratification. The magenta line indicates the location of the vorticity and density profiles shown in figure 4.3.	33
4.3 (a) Time mean meridional component of relative vorticity between 234 and 239 days of model integration, plotted as a function of longitude and depth. Alternating red and blue cells indicate the presence of stacked zonal overturning cells. (b) Density (black line) and time mean meridional component of relative vorticity (grey line) plotted as a function of depth at 90 km west and 250 km south (shown on other figures as a magenta line and point). Vorticity extrema coincide with well mixed regions and zeros with mixing barriers suggesting the density staircases are formed by the overturning cells.	35
4.4 Potential vorticity after 239 days of model integration plotted on (a) the $\sigma = 28.04$ surface, (b) at the equator, (c) at 250 km south of the equator, and (d) at 500 km south of the equator. Black lines show the latitudes at which sections have been plotted. The figures show the advection of anomalous potential vorticity from the northern hemisphere into the southern hemisphere and the excitement of symmetric instability underway. The magenta line and point indicate the location of the vorticity and density profiles shown in figure 4.3.	36

Chapter 1

Introduction

The shape of the sea is always the same. Or rather it's always different, but in the same way. — Philip Marsden

1.1 The Atlantic Meridional Overturning Circulation

- Introduce the AMOC
- Explain how and why it's important
- Talk about how our understanding has changed in recent times
- Not a conveyor but variability and mesoscale features
- Introduce the idea that sub-mesoscale instabilities may play a role
- Talk about water mass formation, transformation, and diapycnal mixing
- Talk about the processes missing from the water mass budget.

1.1.1 *The Western Boundary Current Systems of the Tropical Atlantic*

1.1.2 *The Irminger Current*

1.2 Potential vorticity & symmetric instability

- Describe the character of symmetric instability
- Introduce PV and the instability criteria
- Touch on links to inertial and gravitational instability but direct the reader to chapter 2 for more depth
- Lead into the subsections which describe ways of making potential vorticity negative.

Symmetric instability is a type of submesoscale instability that generates overturning cells in a plane perpendicular to a mean flow. The overturning cells tend to be oriented so that they are parallel to isopycnal surfaces, and so symmetric instability is often said to produce slantwise convection. Although the instability leads to mixing predominantly along isopycnals, it can also induce diapycnal mixing. Secondary shear instabilities further enhance this mixing.

Symmetric instability is intimately linked to the scalar quantity, Ertel potential vorticity. In the ocean this is defined as

$$Q = (\mathbf{f} + \nabla \times \mathbf{u}) \cdot \nabla b \quad (1.1)$$

where \mathbf{f} is the planetary vorticity vector, \mathbf{u} is the velocity field in the rotating frame of reference, and $b = -g \rho / \rho_0$ is the buoyancy field. g is gravitational acceleration and ρ_0 is a constant reference density. One can interpret the potential vorticity as either the component of absolute vorticity normal to isopycnal surfaces and scaled

by the isopycnal thickness, or the stratification along a vortex tube and scaled by the absolute vorticity of the vortex, with the former being the most common way of understanding the quantity.

In a fluid subjected to no momentum or buoyancy forcing, potential vorticity is materially conserved, i.e.

$$\frac{DQ}{Dt} = 0. \quad (1.2)$$

This means if we follow an individual fluid parcel around we expect its potential vorticity to remain constant. This is a fundamental material invariant which arises from a particle relabelling symmetry on isopycnal surfaces in an inviscid fluid (Salmon, 1998).

If a fluid is subject to external or dissipative momentum and buoyancy forcings the conservation of potential vorticity becomes

$$\frac{DQ}{Dt} = \dot{\zeta} \cdot \nabla b + \zeta \cdot \nabla \dot{b} \quad (1.3)$$

where ζ is the absolute vorticity of the field and a \cdot above a quantity represents its material derivative.

A necessary but not sufficient condition for the excitement of symmetric instability is that the vertical component of planetary vorticity and the potential vorticity of a fluid have opposite signs. Mathematically we require that

$$fQ < 0, \quad (1.4)$$

where f is the vertical component of the planetary vorticity vector, also known as the Coriolis parameter. Waters which satisfy this instability criterion are often described as having anomalous potential vorticity.

The overturning cells generated during the excitement of symmetric instability

causes the mixing of waters with anomalous potential vorticity. The momentum and stratification of the fluid are reconfigured by this mixing, producing waters with potential vorticity of approximately zero. This corresponds to the absolute vorticity vector being parallel to isopycnal surfaces.

Consider now a fluid initially stable to symmetric instability. For it to become symmetrically unstable we must make the quantity fQ negative. There are then two distinct ways to generate symmetric instability in such a fluid: the first is to change the sign of the planetary vorticity, and the second is to change the sign of the potential vorticity.

1.2.1 Ekman driven symmetric instability

- can diffusion generate symmetric instability?

1.2.2 Cross equatorial symmetric instability

At the equator planetary vorticity changes from being positive in the northern hemisphere to negative in the southern hemisphere. If we consider a fluid parcel originating in one hemisphere, its potential vorticity will typically match the planetary vorticity so as to ensure symmetric stability. We can then imagine advecting this fluid parcel across the equator. As potential vorticity is materially conserved and planetary vorticity changes sign at the equator, we would expect the symmetric instability criterion to be satisfied in the new hemisphere.

This mechanism does not involve buoyancy or momentum forcing, processes which typically must occur in either a surface or bottom boundary layer. This means symmetric instability resulting from a change in sign of planetary vorticity may occur in the ocean interior and has a distinct character when compared to boundary layer instability. A number of recent observational and theoretical studies have investigated the excitement of symmetric instability resulting from the



Figure 1.1: Caption

cross-equatorial change in sign of planetary vorticity, notably CITATIONS. These studies have, however, focused on weak circulations in the ocean interior as opposed to vigorous western boundary currents. In these western boundary currents there is a constant supply of waters with large magnitude, anomalous potential vorticity. These equatorial western boundary currents are rich with temporally varying features, such as mesoscale eddies which interact differently with symmetric instabilities depending on the flow regime.

Chapter 2

Symmetric instability

In real life there is no algebra — Audrey Horne

This chapter examines symmetric instability and its sub-classifications through several linear instability analyses. This work builds extensively on sections of citep-Goldsworth2021. Sections XXXXX are new.

2.1 Inviscid symmetric instability of parallel shear flow

In this section we will derive some of the classical results concerning the properties of symmetric instability, by considering the stability of an inviscid parallel shear flow on an f -plane. In subsequent sections we will build on this classical analysis to investigate how these properties change in less idealised scenarios.

The Boussinesq equations of motion for a meridionally symmetric, inviscid flow on an f -plane are

$$\frac{Du}{Dt} - fv - \frac{\partial \phi}{\partial x} = 0, \quad (2.1a)$$

$$\frac{Dv}{Dt} + fu = 0, \quad (2.1b)$$

$$\frac{Dw}{Dt} - \frac{\partial \phi}{\partial z} - b = 0, \quad (2.1c)$$

$$\frac{\partial u}{\partial x} + \frac{\partial w}{\partial z} = 0, \quad (2.1d)$$

and

$$\frac{Db}{Dt} = 0. \quad (2.1e)$$

Here, u , v & w are the zonal, meridional & vertical components of velocity, f is the Coriolis parameter, ϕ is the geopotential pressure and b is the buoyancy.

We now consider a flow which is, initially, purely meridional, with $(u, v, w) = (0, V, 0)$, $\phi = \Phi$ and $b = B$. The flow is steady and both geostrophic and hydrostatic balance. Mathematically

$$fV = \frac{\partial \Phi}{\partial x}, \quad (2.2a)$$

$$B = \frac{\partial \Phi}{\partial z}, \quad (2.2b)$$

$$\frac{\partial B}{\partial z} = N^2, \quad (2.2c)$$

and

$$\frac{\partial B}{\partial x} = M^2. \quad (2.2d)$$

We can then perturb this balanced flow, giving perturbed variables $(u, v, w) = (u', V + v', w')$, $\phi = \Phi + \phi'$ and $b = B + b'$. Substituting these values into the equations of motion and considering terms only of linear order or lower in the perturbed variables, we find that

$$\frac{\partial u'}{\partial t} - fv' + \frac{\partial \phi'}{\partial x} = 0, \quad (2.3a)$$

$$\frac{\partial v'}{\partial t} + u' \frac{\partial V}{\partial x} + w' \frac{\partial V}{\partial z} + fu' = 0, \quad (2.3b)$$

$$\frac{\partial w'}{\partial t} + \frac{\partial \phi'}{\partial z} - b' = 0, \quad (2.3c)$$

$$\frac{\partial b'}{\partial t} + w' \frac{\partial B}{\partial z} + u' \frac{\partial B}{\partial x} = 0, \quad (2.3d)$$

and

$$\frac{\partial u'}{\partial x} + \frac{\partial w'}{\partial z} = 0, \quad (2.3e)$$

From equation (2.3e) we see that we can write u' and w' in terms of an overturning streamfunction ψ , where $u' = -\partial_z \psi$ and $w' = \partial_x \psi$. We will now aim to obtain an equation of motion for the overturning streamfunction. The first step is to differentiate the horizontal and vertical momentum equations (equations 2.3a and 2.3c) with respect to the vertical and zonal coordinates respectively. Subtracting the two equations, differentiating with respect to time, and substituting in our equations for $\partial_t b'$ and $\partial_t v'$ gives

$$\frac{\partial^2}{\partial t^2} \left(\frac{\partial^2}{\partial x^2} + \frac{\partial^2}{\partial z^2} \right) \psi + \left(N^2 \frac{\partial^2}{\partial x^2} - 2f \frac{\partial V}{\partial z} \frac{\partial^2}{\partial x \partial z} + f\zeta \frac{\partial^2}{\partial z^2} \right) \psi = 0. \quad (2.4)$$

This equation describes how overturning motions develop within a parallel shear flow, and their dependence on the background flow and its stratification. The equation forms the starting point of Hoskins (1974) and can be used to derive many interesting results relating to symmetric instability (see also Ooyama, 1966).

2.1.1 The instability criterion

In order to derive an instability criterion, Hoskins (1974) uses a trial solution to equation 2.4 of the form $\psi = e^{ik(x \sin \phi + z \cos \phi) + \omega t}$, where ω is the oscillatory frequency of the perturbations, k the wavenumber, and ϕ the angle the perturbation makes with the horizontal. Substituting this into equation 2.4 we find that

$$\omega^2 = \cos^2 \phi (N^2 \tau^2 - 2f \partial_z V \tau + f\zeta), \quad (2.5)$$

where $\tau = \tan \phi$. If ω^2 is less than zero then the corresponding overturning mode will grow exponentially. For this to occur, the discriminant of the quadratic expres-

sion in the above must be negative, i.e. we need $N^2 f \zeta - (f \partial_z V)^2 < 0$. Note that not *all* modes will be unstable if this is the case as the growth rate still depends on the orientation of the perturbations, ϕ . It is true, however, that if $N^2 f \zeta - (f \partial_z V)^2 \geq 0$ all of the overturning modes will be stable. The instability criteria can be simplified somewhat by noting that as the flow under consideration is in geostrophic balance, $f \partial_z V = \partial_x B$, and so we can rewrite the instability criteria as

$$f \left[\left(f + \frac{\partial V}{\partial x} \right) \frac{\partial B}{\partial z} - \frac{\partial V}{\partial z} \frac{\partial B}{\partial x} \right] < 0. \quad (2.6)$$

The term in square brackets is recognisable as the potential vorticity of the background flow and so the classical instability criterion of

$$f Q < 0 \quad (2.7)$$

is recovered.

2.1.2 Orientation of the least stable modes

From equation 2.5 we can see that ω depends on the direction of the perturbation, and so there should be some value of ϕ which maximises the growth rate — i.e. minimises ω^2 . The maxima and minima of ω^2 can be found by differentiating equation 2.5 with respect to ϕ and setting the result to zero. The extrema of ω^2 then satisfy

$$\sin \left(2\phi + \arctan \left(-\frac{2M^2}{N^2 - f\zeta} \right) \right) = 0. \quad (2.8)$$

We can simplify this somewhat if we assume that $|N^2| \gg |f\zeta|$ and that $|N^2| \gg |M^2|$, to give

$$\sin (2(\phi - \phi_{\text{iso}})) = 0, \quad (2.9)$$

where ϕ_{iso} is the angle the isopycnals make to the horizontal. This equation has four solutions, corresponding to ϕ being either parallel or perpendicular to ϕ_{iso} . By evaluating the second order derivative of equation 2.5 we can determine the character of the extrema. We find that with stable stratification, the modes parallel to the isopycnals give minima of ω^2 whereas the modes perpendicular give maxima. Note that the sign of the maxima and minima may be either positive or negative depending on the parameters of the flow, so these modes may be either entirely stable, entirely unstable or a mix of the two.

In the presence of instability, assuming the isopycnal slope isn't "too" steep, and the stratification is stable, the fastest growing mode will be that which is parallel to isopycnals. The growth rate is independent of the magnitude of the wavenumber, however, in the ocean we typically have $|k \sin \phi_{\text{iso}}| \ll |k \cos \phi_{\text{iso}}|$ and so the the fastest growing modes will tend to have a larger horizontal length scale than in the vertical.

2.1.3 Gravitational & inertial instability as limiting cases of symmetric instability

Xu and Clark (1985) explore in detail, how under appropriate coordinate transformations the equations describing the evolution of symmetric instability are mathematically similar to those describing either inertial instability or gravitational instability (an idea first proposed in Hoskins (1974)). This leads to a useful corollary, that symmetric instability is in many ways a hybrid of gravitational and inertial instability (e.g. Haine and Marshall, 1998). To understand this we can perform a simple thought experiment.

Consider a flow, which is free of vertical shear, and therefore has horizontal isopycnals. In this scenario, we have maxima and minima in ω^2 for perturbations which are either purely horizontal or purely vertical. Evaluating ω^2 we find that

the two vertical modes correspond to oscillations (or exponentially growing modes if the stratification is unstable) at the Brunt-Väisälä frequency — this corresponds to gravitational instability. The two horizontal modes correspond to either inertial oscillations or the excitement of inertial instability (depending on the sign of $f\zeta$).

In the limit of weakly sloping isopycnals, symmetric instability becomes equivalent to inertial instability occurring along isopycnals. Another (and slightly less intuitive) interpretation is that it is equivalent to gravitational instability along isolines of absolute vorticity. Both these interpretations can be traced back the interpretation of potential vorticity as either the absolute vorticity normal to an isopycnal surface or the stratification along absolutely vorticity isolines.

2.1.4 Energetics of the instability

The rate of change of the kinetic energy of the perturbations is given by

$$\frac{\partial E_k}{\partial t} = \frac{1}{2} \frac{\partial}{\partial t} (u'^2 + v'^2 + w'^2). \quad (2.10)$$

Substituting in equations 2.3a to 2.3c, we can show that this gives

$$\frac{\partial E_k}{\partial t} = -v'(\mathbf{u}' \cdot \nabla)V - (\mathbf{u}' \cdot \nabla)\phi' + w'b' \quad (2.11)$$

The first term on the right hand side gives the shear production. It corresponds to a transfer of energy from the shear of the mean flow to the turbulent. The term is occasionally split into a “geostrophic” and “lateral” shear production term. Typically the excitement of symmetric instability leads to the excitement of overturning cells oriented along isopycnals, with a horizontal length scale much greater than the vertical. If the turbulent motion is along isopycnals then this term can be thought of as an extraction of energy from the along isopycnal shear of the mean flow.

The second term on the right hand side is the turbulent pressure work term. Using incompressibility of the turbulent flow we can show that

$$-(\mathbf{u}' \cdot \nabla) \phi' = -\nabla \cdot (\mathbf{u}' \phi') . \quad (2.12)$$

This leads to the interpretation of the pressure work term as being a flux. Due to the no normal flow boundary condition, we know this flux must be zero at the boundaries, and all this term does is advect turbulent kinetic energy around the domain, rather than increase the total turbulent kinetic energy. As such it's relatively boring and we won't consider it any further.

The final term in equation 2.10 is the turbulent buoyancy flux and corresponds to the turbulent flow extracting gravitational potential energy from the advection of buoyancy anomalies.

2.1.5 *The classical and energetic definitions of symmetric instability*

In the above (and in what follows), we have been referring to the overturning instability that occurs when the potential vorticity of a flow has the opposite sign to the planetary vorticity. We refer to this as the *classical* definition of symmetric instability, as proposed by Hoskins (1974). Under this definition, gravitational and inertial instability are both special cases of symmetric instability.

This isn't, however, the only definition of symmetric instability. Thomas et al. (2013) propose a more fine-grained approach to the taxonomy of these instabilities, in which they can be distinguished by their energy source and the source of their anomalous potential vorticity. They define symmetric instability as getting its energy from the geostrophic shear of the mean flow, inertial instability as getting its energy from the lateral shear of the mean flow and gravitational instability as getting its energy from buoyancy fluxes. Under these definitions we can have

any of pure inertial, hybrid inertial symmetric, pure symmetric, hybrid symmetric gravitational, and pure gravitational instabilities. We refer to this as the *energetic* definition of symmetric instabilities.

For the purposes of this work we adopt the classical definition. This is a purely aesthetic choice — we enjoy the simplicity of the definition and how it preserves the link between symmetric instability, pure gravitational and pure inertial instabilities, potential vorticity, and the extraction of turbulent kinetic energy from along isopycnal shear.

2.2 Inviscid symmetric instability of axisymmetric flow

Parallel shear flow in geostrophic balance is a good first order approximation of a western boundary current’s velocity structure. These current systems are often unstable to a myriad of other instabilities, however, and the “background” flow is rarely as simple as a parallel shear flow. In the North Brazil Current for instance, we see the spinning up of the North Brazil Current rings — huge anticyclonic eddies resulting from barotropic instability — a few degrees North of the equator. With this in mind, we can see how it might be useful to examine how symmetric instability changes when the background flow is that of an eddy rather than that of a western boundary current.

To first order, we can think of eddies as axisymmetric vortices in cyclo-geostrophic balance. The natural coordinate system for such a flow is cylindrical polars, and we can assume symmetry along the azimuthal direction. It is possible to write out the Boussinesq equations of such a flow and linearise them with respect to axisymmetric perturbations. We can then manipulate the equations in order to find an analogue of equation 2.4 for an axisymmetric flow. The resulting equation, however, is nowhere near as elegant, due to the considerably more complex form of ∇

in cylindrical polar coordinates and the presence of centrifugal forces¹. Thankfully, the revised instability condition, as derived in Buckingham et al. (2021), *is* just as elegant, and is given by

$$\left(f + \frac{2V_\phi}{r} \right) Q < 0. \quad (2.13)$$

Consider now an anticyclone, meaning the term $2V_\phi/r$ has opposite sign to f . If the anticyclone is sufficiently strong, then planetary vorticity will be overwhelmed by the vorticity of the vortex, and flows with potential vorticity opposite in sign to the planetary vorticity will still be stable to symmetric instability. Thus we see that anticyclonic vortexes are more robust to symmetric instability than the classical instability criterion suggests.

To see this more clearly we can analyse the dispersion relation, given by

$$\omega^2 = \cos^2 \phi \left(N^2 \tau^2 - 2 \left(f + \frac{2V_\phi}{r} \right) \partial_z V \tau + \left(f + \frac{2V_\phi}{r} \right) \zeta \right). \quad (2.14)$$

We can see that this is identical to equation 2.5 which gives the dispersion relation for the case of parallel shear flow, but with the Coriolis parameter f replaced by $f + 2V_\phi/r$. Here we can see how the curvature doesn't even need to overwhelm the planetary vorticity to reduce the growth rate of symmetric instability.

- Explain parallel shear flow like a western boundary current and axisymmetric flow like an eddy
- Derive the instability criteria
- Look at a Rankine vortex type flow
- Explain stabilising and destabilising forces of rotation

¹A full derivation of the axisymmetric analogue is given in appendix A of Buckingham et al. (2021).

- Suggest we expect eddy cores to be more stable than outer shells

2.3 Viscous inertial instability

citet{Hoskins1974} shows that an inviscid meridional jet, initially in thermal wind balance and symmetric about the meridional axis, may be linearly unstable and produce overturning in the x - z plane. The overturning can be represented as a streamfunction, ψ , where the zonal and vertical velocities are given by $u = -\partial_z \psi$ and $w = \partial_x \psi$ respectively. citet{Hoskins1974} shows that the streamfunction, to terms linear in ψ , satisfies the partial differential equation

$$\frac{\partial^2}{\partial t^2} \left(\frac{\partial^2}{\partial x^2} + \frac{\partial^2}{\partial z^2} \right) \psi + \left(N^2 \frac{\partial^2}{\partial x^2} - 2f \frac{\partial V}{\partial z} \frac{\partial^2}{\partial x \partial z} + f \zeta \frac{\partial^2}{\partial z^2} \right) \psi = 0. \quad (2.15)$$

Here N is the buoyancy frequency which is assumed to be constant, f is the planetary vorticity, V is the basic state meridional velocity, and ζ is the absolute vorticity of the basic state about the vertical. The equation is easily generalized to flows with a harmonic vertical viscosity, by replacing ∂_t with $\partial_t - A_r \partial_{zz}^2$, where A_r is the vertical viscosity.

Solving for ψ in the viscous case is a difficult problem; however, much can be gained by considering a basic flow that is both barotropic and meridional. Thus the term proportional to the vertical shear of the meridional flow is set to zero. The resulting equation is

$$\left(\frac{\partial}{\partial t} - A_r \frac{\partial^2}{\partial z^2} \right)^2 \left(\frac{\partial^2}{\partial x^2} + \frac{\partial^2}{\partial z^2} \right) \psi + \left(N^2 \frac{\partial^2}{\partial x^2} + f \zeta \frac{\partial^2}{\partial z^2} \right) \psi = 0, \quad (2.16)$$

which, strictly speaking, describes the evolution of an inertial instability due to the flow being free of vertical shear.

We can now try to find solutions of the form $\psi(x, z, t) = \hat{\psi}(x) e^{i(mz - \omega t)}$. Substi-

tuting this into (2.16), we obtain the following boundary value problem:

$$\frac{(\hat{\omega}^2 - N^2)}{m^2} \frac{d^2 \hat{\psi}}{dx^2} + f\zeta \hat{\psi} = \hat{\omega}^2 \hat{\psi}, \quad (2.17)$$

where $\hat{\omega} = \omega + iA_r m^2$. Upon appropriate non-dimensionalisation of the coordinates and variables, (2.17) is identical to equation 4 of [citetPlougonven2009](#), who identify it as a Schrödinger equation.

From the work of Hoskins (1974), it is known that in the inviscid limit, $\hat{\omega}^2 \sim f^2$. For oceanic western boundary flows, typically $N^2 \gg f^2$. This means we can make the approximation $N^2 - \hat{\omega}^2 \approx N^2$. Plougonven and Zeitlin (2009) show that this is equivalent to making the hydrostatic approximation and that, for a flow similar to the one considered here, there is a negligible effect on the solutions. After making the hydrostatic approximation, we are then left with

$$-\frac{N^2}{m^2} \frac{d^2 \hat{\psi}}{dx^2} + f\zeta \hat{\psi} \approx \hat{\omega}^2 \hat{\psi}. \quad (2.18)$$

The eigenfunctions of the equation are $\hat{\psi}$. They define the horizontal structure of the overturning streamfunction. The eigenvalues of the equation are $\hat{\omega}^2$. If the eigenvalue is negative, then it is possible for ω to be imaginary. If ω is imaginary, then the overturning circulation may either grow or decay exponentially. It is useful to introduce the quantity $\sigma = \text{Im}(\omega)$, which, if positive, corresponds to the exponential growth rate; if negative it gives the decay rate. The value of σ is maximized for the smallest real eigenvalue of equation 2.18. For each eigenfunction, there exists a spectrum of vertical wave-numbers, each with a characteristic growth rate (or frequency if stable). The relationship between the growth rate and the vertical wavenumber is determined by the eigenvalue, $\hat{\omega}$.

To calculate the eigenfunctions and eigenvalues of the equation, we must first specify a buoyancy frequency and velocity profile, from which vorticity can be cal-

culated. As we are interested in western boundary currents, we will consider an idealized meridional flow: the barotropic Bickley jet. The velocity of the jet can be expressed as

$$V(x) = V_0 \left(1 - \tanh^2 \left(\frac{x - x_{\text{mid}}}{\delta_b} \right) \right) \quad (2.19)$$

where V_0 is the peak velocity of the jet, x is the across stream coordinate, x_{mid} gives the distance of the peak velocity of the jet from the western boundary and δ_b is the width of the jet. The jet is symmetric in the along stream direction. The jet parameters are set as follows: $V_0 = 0.87 \text{ m s}^{-1}$, $x_{\text{mid}} = 40 \text{ km}$ and $\delta_b = 30 \text{ km}$. The parameters are chosen to be similar to those used in the two-dimensional and three-dimensional numerical models described in sections ?? and ?? at a depth of 200 m. These parameters are, in turn, loosely based on what is seen in the North Brazil Current citepJohns1998. The velocity profile used is shown in figure ???. In the northern hemisphere, we would expect to see symmetric instability develop in a region to the right of the jet's center. In the southern hemisphere, we may expect to see symmetric instability between the western boundary and the jet's center. In such a configuration, the western boundary would input anomalous vorticity into the flow, something that this idealized framework is unable to represent. For this reason, and the fact that this study focuses on cross-equatorial flows, we do not apply the linear stability analysis to northward flowing jets in the southern hemisphere.

The buoyancy frequency is set to a value of $5 \times 10^{-3} \text{ s}^{-1}$, which is the mean buoyancy frequency at a depth of between 200 m and 400 m, as estimated from 82 neutral density density profiles taken by an Argo float off the coast of Brazil between January 2016 and February 2017 citepArgo2019. The trajectory of the float and the mean neutral density profile are shown in figure ???. The use of neutral density in calculating the buoyancy frequency means the results of the linear stability analysis will be more applicable to what is seen in the models presented in the following

sections rather than the ocean. This is because the neutral density calculation does not reliably preserve vertical buoyancy gradients citepEden1999. Data from a single Argo float was used as it was readily available and provides a plausible estimate of the density structure of the region. The value of f is set to $1.01 \times 10^{-5} \text{ s}^{-1}$, corresponding to a latitude of approximately 4°N .

For each eigenfunction, which physically corresponds to the horizontal structure of the overturning cell, we can plot the growth rate, σ , as a function of vertical wavenumber, m , and vertical viscosity, Λ_r . This is done in figure ???. We find that, for a given vertical viscosity, there is a value of the vertical wavenumber which maximizes the growth rate. As the growth is exponential, within a few e-folding timescales, the vertical mode which maximizes σ will dominate the structure of the instability — assuming non-linear effects have not taken hold before this time. Thus, although a discrete set of horizontal modes and a continuous spectrum of vertical modes may be excited, we may expect a single horizontal and vertical mode to dominate the structure of the instability. However, we can only verify this expectation with the use of a numerical model which takes into account the non-linearities neglected here.

Below a maximum ‘critical’ viscosity, there is a maximum and minimum vertical wavelength at which unstable modes exist; at higher viscosities, all modes are stable. The maximum wavelength is a result of stratification inhibiting vertical motions. Any mode with a wavelength smaller than the minimum will experience strong viscous damping, rendering the mode stable. The minimum vertical wavelength tends to zero in the inviscid limit. The maximum ‘critical’ viscosity is found when the maximum wavelength allowed by the stratification and the minimum wavelength allowed by viscosity are equal.

It is not *a priori* clear whether the viscosity we are interested in should be a molecular or turbulent viscosity. If one is looking for signs of symmetric instabil-

ity in a sufficiently coarse ocean model, then it is the turbulent viscosity that will set the vertical length scale. This makes sense as it is the only viscosity the fluid is ‘aware’ of. For real fluids, matters become more problematic. citet{Griffiths2003a} suggests that secondary Kelvin-Helmholtz instabilities form as a result of symmetric instability and play a more dominant role in the vertical scale selection than does viscosity. This means that the findings of this linear-stability analysis apply to the results of numerical models which fail to resolve these secondary instabilities, but the relation to what might be observed in meridional western boundary flows in the ocean is more ambiguous.

For a given vertical viscosity we can also plot the two-dimensional structure of the overturning that the instability generates, as shown in figure ?? for a viscosity of $4 \times 10^{-4} \text{ m}^2 \text{ s}^{-1}$ (this viscosity was chosen as it corresponds to the value used in the numerical models presented in sections 3 & 4). We see that the instabilities generate a stack of alternating overturning cells. Overlain in the figure is the absolute vorticity (solid line), highlighting that the cells are strongly localized to the region of negative potential vorticity. Despite the localization, the overturning is non-zero outside of the region of negative absolute vorticity. This enables the mixing of waters with positive and negative PV, which over time will create a neutrally stable PV configuration.

The mode shown in figure ?? has an e-folding timescale of around 2 days. Seawater has a viscosity of $10^{-6} \text{ m}^2 \text{ s}^{-1}$, which would lead to overturning cells with a much smaller vertical wavelength of 15 m and a smaller e-folding time scale of approximately 1 day. That the timescale is decreased slightly when using a realistic viscosity suggests that the instability will be at least as efficient at neutralizing anomalous PV in the ocean. Differences between the vertical lengthscales seen here and in other works citep[e.g.][]Taylor2009 can be understood in terms of the dependence on vertical viscosity, and the artificially high ‘eddy viscosity’ used

here.

A more rigorous analysis of the solutions to the boundary value problem described in this section is given in [citetPlougonven2009](#), who consider barotropic zonal shear flows on an f -plane. On an f -plane there is no physical distinction between meridional and zonal flows so their findings are broadly applicable, although the vorticity profiles they use differ from those considered here. There also exists a broad literature base on linear stability analyses of symmetric and inertial instabilities on a β -plane, with a focus on zonal currents (e.g. Kloosterziel et al., 2017; Ribstein et al., 2014; Griffiths, 2003; Hua et al., 1997).

2.4 Viscous symmetric instability with the complete Coriolis force

Zeitlin (2018) states that “symmetric instability drastically changes upon inclusion of the full Coriolis force.” The author goes on to perform a linear stability analysis of a zonally symmetric shear flow on an f -plane, taking into account the non-traditional component of the full Coriolis force. They find that the growth rate and spatial structure of unstable modes may be significantly altered by inclusion of the full Coriolis force. Naïvely, one may expect to observe drastic changes in the above numerical simulations, given that on an ordinary f -plane there is no difference between a meridional and zonal flow (as the system has no preferred orientation). However, the inclusion of the non-traditional component of the Coriolis force breaks this symmetry and reintroduces a natural meridional direction. To understand how symmetric instability in meridional flows changes under the complete Coriolis force, we must repeat the linear stability analysis of Zeitlin (2018) but for the case of a meridional flow.

The Boussinesq equations of motion for a meridionally symmetric flow on an

f -plane, with the complete Coriolis force, and in the limit in which the horizontal length scale is much larger than the vertical length scale, are

$$\frac{Du}{Dt} - fv + F_{NT}w - \frac{\partial \phi}{\partial x} = A_r \frac{\partial^2}{\partial z^2} u, \quad (2.20a)$$

$$\frac{Dv}{Dt} + fu = A_r \frac{\partial^2}{\partial z^2} v, \quad (2.20b)$$

$$\frac{Dw}{Dt} - F_{NT}u - \frac{\partial \phi}{\partial z} - b = A_r \frac{\partial^2}{\partial z^2} w, \quad (2.20c)$$

$$\frac{\partial u}{\partial x} + \frac{\partial w}{\partial z} = 0, \quad (2.20d)$$

and

$$\frac{Db}{Dt} = \kappa \frac{\partial^2}{\partial z^2} b, \quad (2.20e)$$

where, A_r is the viscosity, κ is the buoyancy diffusion coefficient and F_{NT} is the non-traditional component of the Coriolis parameter.

Similarly to section 2.1 we will now consider a flow which is, initially, purely meridional, with $(u, v, w) = (0, V, 0)$, $\phi = \Phi$ and $b = B$. The flow is steady, in geostrophic balance and hydrostatically balanced. Mathematically

$$fV = \frac{\partial \Phi}{\partial x}, \quad (2.21a)$$

$$B = \frac{\partial \Phi}{\partial z}, \quad (2.21b)$$

$$\frac{\partial B}{\partial z} = N^2, \quad (2.21c)$$

$$\frac{\partial^2 B}{\partial z^2} = 0. \quad (2.21d)$$

$$\frac{\partial B}{\partial x} = M^2, \quad (2.21e)$$

and

$$\frac{\partial^2 V}{\partial z^2} = 0. \quad (2.21f)$$

Again, we will perturb this balanced flow, giving perturbed variables $(u, v, w) = (u', V + v', w')$, $\phi = \Phi + \phi'$ and $b = B + b'$. Substituting these values into the equations of motion and considering terms only of linear order or lower in the perturbed variables, we find that

$$\frac{\partial u'}{\partial t'} + F_{NT}w' - fv' + \frac{\partial \phi'}{\partial x} = 0, \quad (2.22a)$$

$$\frac{\partial v'}{\partial t'} + u' \frac{\partial V}{\partial x} + w' \frac{\partial V}{\partial z} + fu' = 0, \quad (2.22b)$$

$$\frac{\partial w'}{\partial t'} + \frac{\partial \phi'}{\partial z} - b' - F_{NT}u' = 0, \quad (2.22c)$$

$$\frac{\partial b'}{\partial t} - \kappa \frac{\partial^2 b'}{\partial z^2} + w' \frac{\partial B}{\partial z} + u' \frac{\partial B}{\partial x} = 0, \quad (2.22d)$$

and

$$\frac{\partial u'}{\partial x} + \frac{\partial w'}{\partial z} = 0, \quad (2.22e)$$

where the operator $\partial/\partial t'$ is defined as

$$\frac{\partial}{\partial t'} = \frac{\partial}{\partial t} - A_r \frac{\partial^2}{\partial z^2}. \quad (2.23)$$

From equation 2.22e we see that we can again write u' and w' in terms of an overturning streamfunction ψ , where $u' = -\partial_z \psi$ and $w' = \partial_x \psi$. We can then attempt to find an equation of motion for the streamfunction, analogous to equation 2.4. As before, we differentiate the zonal and vertical momentum equations (equations 2.22a and 2.22c) with respect to the vertical and zonal coordinates re-

spectively and then subtract them, giving

$$\frac{\partial}{\partial t'} \left(\frac{\partial^2}{\partial x^2} + \frac{\partial^2}{\partial z^2} \right) \psi - f \frac{\partial v'}{\partial z} + \frac{\partial b'}{\partial x} + F_{NT} \left(\frac{\partial u'}{\partial x} + \frac{\partial w'}{\partial z} \right) = 0. \quad (2.24)$$

We note that the only place F_{NT} enters this equation is in the final term, and that because of the continuity equation (equation 2.22e) this term is equal to zero. If we now differentiate the above with respect to t' and substitute in the equations for $\partial_{t'} b'$ and $\partial_{t'} v'$ we get

$$\frac{\partial^2}{\partial t'^2} \left(\frac{\partial^2}{\partial x^2} + \frac{\partial^2}{\partial z^2} \right) \psi + \left(N^2 \frac{\partial^2}{\partial x^2} - 2f \frac{\partial V}{\partial z} \frac{\partial^2}{\partial x \partial z} + f \zeta \frac{\partial^2}{\partial z^2} \right) \psi = 0. \quad (2.25)$$

which apart from the viscous terms is identical to equation 2.4². This has absolutely no dependence on F_{NT} at all and from this we conclude that the complete Coriolis force does not alter symmetric instability in meridional, parallel shear flows. This finding is not in any way contradictory to the findings of Zeitlin (2018). The difference arises due to the asymmetry between the purely meridional flow considered here and the zonal flow considered in the aforementioned study.

It is, in fact, possible to make a more general statement about the types of forces which do not alter the evolution of meridional symmetric instabilities. We can modify the momentum equations (2.3a and 2.3c) with the addition of any irrotational force acting in the xz -plane and which satisfies the relationship

$$\frac{\partial \mathcal{F}_x}{\partial z} + \frac{\partial \mathcal{F}_z}{\partial x} = 0, \quad (2.26)$$

where \mathcal{F}_x and \mathcal{F}_z are the zonal and meridional components of the force respectively. This can be understood in the framework of Marshall and Pillar (2011) as follows — an irrotational force is divergent and so will project on to the pressure gradi-

²Here we have set $\kappa = A_r$. This is done to simplify the notation and the arguments subsequently made do not lose their generality.

ent terms of the momentum equation. A rotational force is non-divergent and so projects entirely onto the acceleration term. An irrotational (divergent) force is not able to alter the acceleration term. In the system described above, the inclusion of the complete Coriolis force may alter the pressure field but not the motions within the xz -plane due to its irrotational nature.

Although the crossing of the equator is a meridional phenomenon, western boundary currents, such as the North Brazil Current or the deep western boundary current, will be oriented at some angle to a meridian, and so have both zonal and meridional components of velocity. In the zonal limit, symmetric instability can change drastically with the inclusion of the full Coriolis force, whereas in the meridional limit there is no change at all. For a realistic (not purely meridional) western boundary current crossing the equator, the structure of symmetric instability may therefore have some dependence on the complete Coriolis force.

The relative importance of non-traditional effects depends on the direction of the current relative to the meridional direction. For a current oriented at an angle θ to the meridional direction, the findings of Zeitlin (2018) apply but with the value of F_{NT} scaling with $\sin \theta$. Zeitlin (2018) defines a “non-traditionality” parameter and using the findings of our work we can generalise it to flows with a meridional component giving

$$\gamma = \frac{\cot \phi \sin \theta H}{L} \quad (2.27)$$

where γ is the “non-traditionality parameter” and ϕ is the latitude. Non-traditional effects are important when $\gamma \sim 1$. Close to the equator, the coast of Brazil forms an angle of $\theta \sim 60^\circ$ to the meridian. From work that will be discussed in subsequent chapters, we suspect symmetric instability in the North Brazil Current to occur at a latitude of around 4°N , and the current has $H \sim 100$ m and $L \sim 30$ km giving $\gamma \sim 0.04$. This suggests that non-traditional effects are unlikely to be hugely important in the North Brazil Current. For the deep western boundary current we expect

$\phi \sim 1^\circ\text{N}$, $H \sim 1,000$ m and $L \sim 50$ km. This gives $\gamma \sim 1$ suggesting non-traditional effects may be important here. Finally, the Irminger current sits at around 60°N , forms an angle of $\theta \sim 30^\circ$ to the meridian, has $H \sim 100$ m and $L \sim 30$ km. Due to its high latitude we suspect non-traditional effects will be very weak, and this is reflected in a value of $\gamma \sim 10^{-3}$.

Chapter 3

Symmetric instability in a cross-equatorial surface current

Brrrrrrr — Fraser Goldsworth

This chapter focuses on work first published in ?.

Chapter 4

Symmetric instability in a cross-equatorial deep western boundary current

Brrrrrrr — Fraser Goldsworth

4.1 Introduction

Density staircases are step like features which can be seen in plots of seawater density against depth, and they are ubiquitous in the global ocean Stern (1960); Schmitt et al. (1987); Melling et al. (1984); Tait and Howe (1968); Johannessen and Lee (1974); Lambert and Sturges (1977),. The staircases consist of alternating well mixed regions with low stratification, and thin interfaces with high stratification. The high stratification interfaces can form “mixing barriers” which inhibit the vertical transport of water properties such as heat and salt, whereas mixing is enhanced in the well mixed regions. This can affect both diapycnal mixing and water mass transformation rates Schmitt et al. (2005). Many staircases form as a result of double diffusion convection, a mechanism which requires certain conditions regarding the saline stratification relative to the thermal stratification to be met Merryfield (2000). Other staircase generation mechanisms exist, for example

inhomogeneous mixing Balmforth et al. (1998).

The Atlantic meridional overturning circulation (AMOC) is a global scale circulation that is important in transporting heat and salt both laterally and vertically, including between hemispheres Jackson et al. (2015). There are two important cross-equatorial components to the AMOC – the northward flowing, surface intensified North Brazil Current, and the southward flowing deep western boundary current Bower et al. (2019). At 5°S the deep western boundary current transports 25.5 ± 8.3 Sv, sits between 1,200 m and 3,600 m below the surface, with a width of approximately 100 km and a peak velocity of around 20 cm s^{-1} Schott et al. (2005). ? show that cross-equatorial western boundary currents such as this may be susceptible to symmetric instability.

Symmetric instability is a type of sub-mesoscale instability which occurs when the Ertel potential vorticity of a flow has the opposite sign to the planetary vorticity Stone (1966); Hoskins (1974). Potential vorticity is defined as

$$Q = (\mathbf{f} + \nabla \times \mathbf{u}) \cdot \nabla b, \quad (4.1)$$

where \mathbf{f} is the planetary vorticity vector, \mathbf{u} is the velocity field of the flow $b = -g\rho/\rho_0$ is the buoyancy field. Potential vorticity with sign opposite to that of the (vertical component of) planetary vorticity is often described as anomalous. Symmetric instability may be excited in cross-equatorial flows as potential vorticity is materially conserved, whereas at the equator planetary vorticity changes sign. This means fluid originating from the northern hemisphere which has positive potential vorticity (in order for the flow to be stable to symmetric instability) may become symmetrically unstable upon crossing the equator, as planetary vorticity is negative in the southern hemisphere ?. The excitement of symmetric instability creates stacked overturning cells in the plane perpendicular to the flow. These

overturning cells act to set the potential vorticity of the flow to zero. Potential vorticity of zero is often described as being marginal.

Anomalous potential vorticity can be generated in one of two ways, either by changing the sign of the potential vorticity or by changing the sign of the planetary vorticity. As potential vorticity is materially conserved, a fluid may only change the sign of its potential vorticity via frictional momentum forcing or diabatic buoyancy forcing. These processes typically alter only the local potential vorticity and occur in boundary layers, meaning symmetric instability tends to be confined to either the surface boundary layer or the sloping bottom boundary layer. A change in sign of planetary vorticity, however, generates anomalous potential vorticity throughout the water column. This makes cross-equatorial symmetric instability distinct from instabilities generated by potential vorticity forcing. A host of recent studies have identified regions where cross-equatorial symmetric instability may be excited ?Forryan et al. (2021); Zhou et al. (2022); Jakoboski (2019). In this paper we will investigate the excitement of symmetric instability in a cross-equatorial deep western boundary current, away from the surface and frictional bottom boundary layers.

In section 4.2 an idealised numerical model of a deep western boundary current crossing the equator is described. In section 4.3 we show that the model output shows signs of density staircases and the excitement of symmetric instability, and propose that the staircases are generated as a result of the symmetric instability's excitement. Finally, in section 4.5 we summarise our findings and outline our plans for future work.

4.2 Methods

Simulations of an idealised Deep Western Boundary Current crossing the equator were performed using the MITgcm, checkpoint 68i, on the ARCHER2 HPC facility. The domain size is 600 km in the zonal, 3,600 km in the meridional and 4,500 m in the vertical. The horizontal grid spacing is 1 km and the vertical grid spacing 10 m. The time-step is 144 s and the model is integrated for a total of 239 days. The model domain is sited on a β -plane, with the equator placed 2,000 km north of the southern boundary. β is set to $2.3 \times 10^{-11} \text{ s}^{-1} \text{ m}^{-1}$, and the non-traditional Coriolis parameter to $1.5 \times 10^{-4} \text{ s}^{-1}$.

At the surface a rigid lid boundary condition is employed. The lateral boundary condition is set to be free-slip and the bottom boundary condition to no-slip. The model has sloping bathymetry which can be seen in figure 4.1b. The model is initialised by setting the meridional velocity and density profile to those shown in figure 4.1b, and with a zonal velocity of zero. The model is forced by prescribing the meridional velocity, zonal velocity, and the density, at the northern and southern domain boundaries. The same fields used to initialise the model are used as boundary conditions. A sponge is placed at the northern and southern edges of the domain. The northern sponge is 100 km thick and the southern sponge 300 km thick. The inverse relaxation time-scale varies from $1 \times 10^{-5} \text{ s}^{-1}$ (corresponding to a time scale of around 1.2 days) at the outer boundaries to 0 at the inner. The inverse relaxation time-scale has a tanh shape, with a characteristic length-scale of 5 km in the northern sponge and 10 km in the southern.

A linear equation of state is used, with a reference density of $1022.73 \text{ kg m}^{-3}$ and thermal expansion coefficient of $2 \times 10^{-4} \text{ K}^{-1}$. The thermal diffusion coefficient is set to $1 \times 10^{-5} \text{ m}^2 \text{ s}^{-1}$. A second order-moment Prather with flux limiter advection scheme was used. Salinity was set to zero throughout the model.

Momentum dissipation is provided by a vertical Laplacian viscosity of $4 \times 10^{-4} \text{ m}^2 \text{ s}^{-1}$ and an adaptive biharmonic Smagorinsky viscosity.

Model configuration files and processed outputs are available from [?](#) and [?](#). The subsequent analysis made heavy use of the open source xarray [?](#) and Dask [?](#) software libraries. Potential vorticity was calculated using the algorithm of Morel et al. (2019).

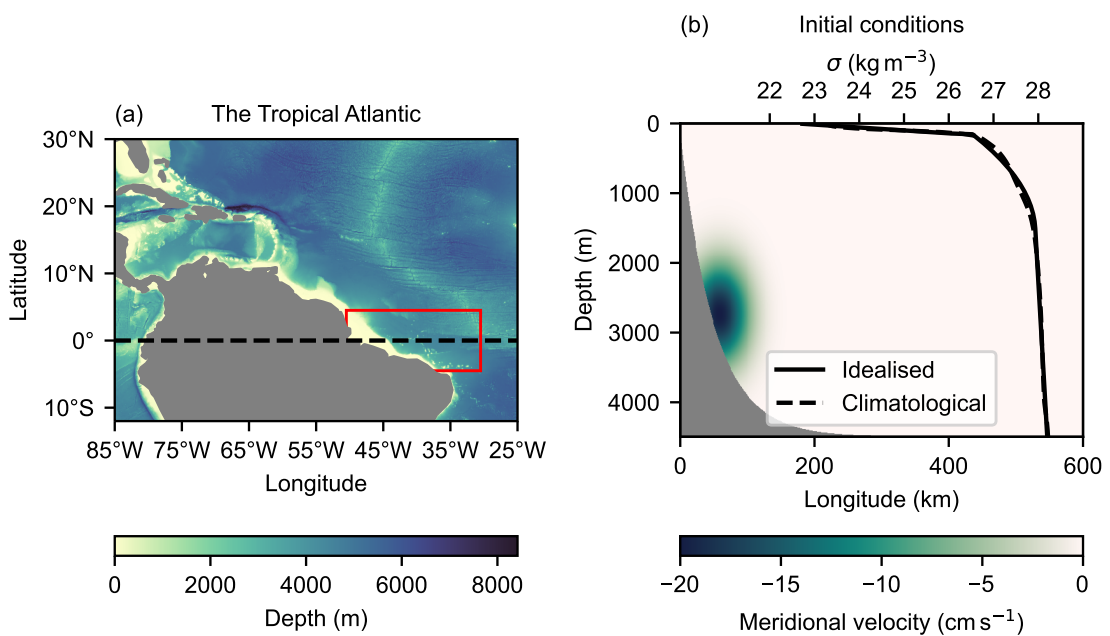


Figure 4.1: (a) A map of the tropical Atlantic and its bathymetry. Climatological profiles of neutral density were aggregated from the area enclosed by the red rectangle. Bathymetry data from [?](#). (b) Initial meridional velocity profile and density profile (solid line) used as initial conditions and boundary conditions for the model. The velocity profile is based on observations by Schott et al. (2005), and the density profile on the climatological mean (dashed line) ([?](#)).

4.3 Results & discussion

Figure 4.2b shows the squared buoyancy frequency in the model after 239 days of integration at 250 km south. Immediately apparent are the thin, sharp regions of high stratification (so called “mixing barriers”) separating larger regions of well mixed waters with low and uniform stratification. Moving to 500 km south, we see in figure 4.2c that some of the weaker barriers have dissipated, however the stronger barriers remain. Figure 4.2a shows the squared buoyancy frequency at the equator. Towards the right of the current’s core we see some weak mixing barriers.

Figure 4.3a shows the average of the meridional component of relative vorticity 250 km south of the equator between 234 and 239 days of model integration. This can be thought of as a crude proxy for a zonal overturning streamfunction. We consider it here as the true zonal overturning streamfunction is ill-defined, since the flow is not invariant in the meridional direction. Looking at the vorticity as akin to a streamfunction, we see that there are a series of counter-rotating stacked overturning cells between around 1,750 m and 3,500 m below the surface. Comparing with figure 4.2b we see that the structure of the buoyancy frequency squared and the meridional vorticity are remarkably similar, with the horizontal edges of the overturning cells (vorticity zeros) approximately coinciding with the locations of the mixing barriers. This is shown more clearly in figure 4.3b. The black line shows σ plotted as a function of depth at 250 km south and 90 km west (the location of the magenta lines and points shown in the other figures). The grey line shows the meridional component of relative vorticity at the same point. Both quantities have been averaged over the time period spanning 234 to 239 days. The treads of the steps in σ correspond to mixing barriers and the risers to well mixed regions. When comparing σ and the meridional vorticity we again see that the mixing barriers tend to coincide with vorticity zeros, whereas the mixing barriers coincide

with vorticity extrema. This suggest that the inhomegeneous mixing driven by the overturning cells is what is causing the formation of the staircases.

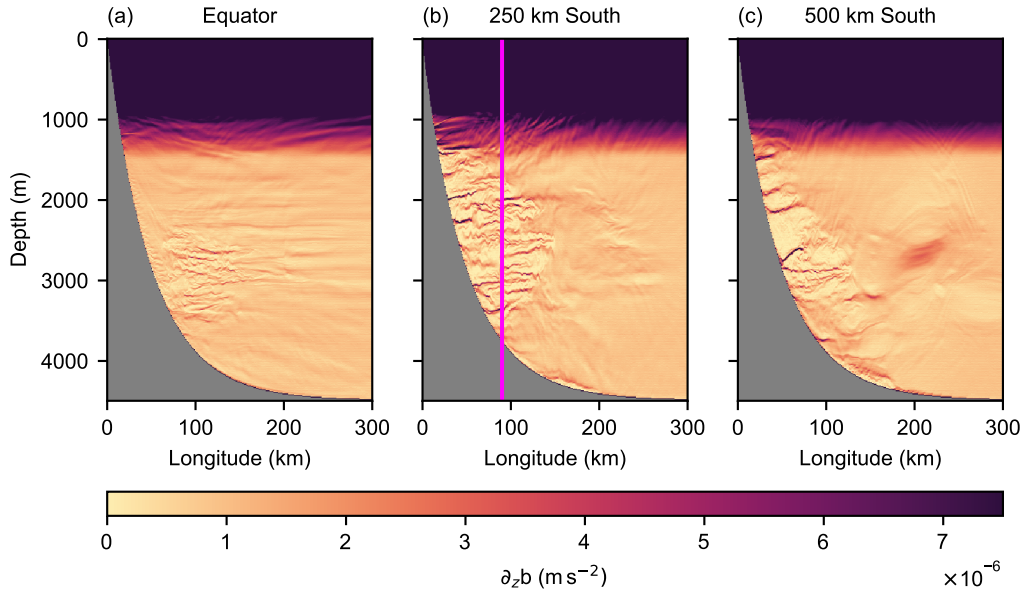


Figure 4.2: Squared buoyancy frequency after 239 days of model integration plotted at (a) 250 km south of the equator, (b) 500 km south of the equator and (c) 600 km south of the equator. The figures show the presence of mixing barriers (thin filaments of strong stratification) separated by well mixed regions of low stratification. The magenta line indicates the location of the vorticity and density profiles shown in figure 4.3.

We believe that the overturning cells are generated by symmetric instability and that it is this overturning that goes on to generate the density staircases, as opposed to the density staircases somehow inducing overturning. Previous work by ? has demonstrated that western boundary currents can become unstable when crossing the equator as they advect anomalous potential vorticity from one hemisphere into the other. In figure 4.4a, which shows the potential vorticity on the $\sigma = 28.04$ surface, we can see the advection of positive potential vorticity from the northern hemisphere into the southern hemisphere, meaning we may expect to

see symmetric instability excited south of the equator. The excitement of the instability is apparent in a region from around 25 km to 600 km south of the equator. Figures 4.4b, c, and d show the potential vorticity as a function of depth and longitude at, the equator, 250 km south and 500 km south respectively, after 239 days of model integration. At the equator we see the advection of waters with anomalous potential vorticity into the southern hemisphere. At 250 km south we can see the excitement of symmetric instability, and by 500 km south we can see large pools of neutral potential vorticity suggesting the waters here have experienced symmetric instability, with the excitement of symmetric instability still underway at around 3,000 m of depth. In figure 4.4b we also see symmetric instability like patterns in a region of negative potential vorticity. This suggests these waters with negative potential vorticity were undergoing symmetric instability in the northern hemisphere before being advected south of the equator. This also explains the presence of the weak staircases at the equator seen in figure 4.2a.

Unlike in the study of ?, we see the excitement of symmetric instability close to the equator followed by the formation of eddies, whereas in the former study we see the spinning up of large anti-cyclonic eddies followed by the excitement of symmetric instability further away from the equator. This is due to the reduced growth rate of barotropic instability in the deep western boundary current, meaning that symmetric instability dominates over short time-scales. This is further exacerbated by the anti-cyclonic eddies seen by ?, which act to reduce the growth rate of the symmetric instability in their experiments, allowing anomalous potential vorticity to persist whilst the eddies grow Buckingham et al. (2021).

4.4 A simplified model of stircse formation

$$\frac{\partial b}{\partial t} = -u \frac{\partial b}{\partial x} - w \frac{\partial b}{\partial z} + \kappa \frac{\partial^2 b}{\partial z^2} \quad (4.2)$$

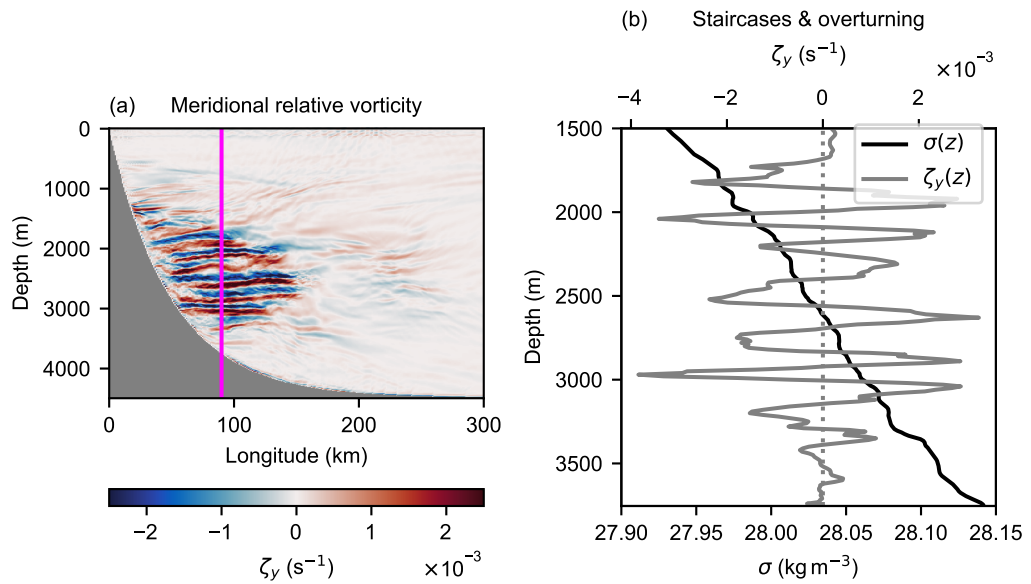


Figure 4.3: (a) Time mean meridional component of relative vorticity between 234 and 239 days of model integration, plotted as a function of longitude and depth. Alternating red and blue cells indicate the presence of stacked zonal overturning cells. (b) Density (black line) and time mean meridional component of relative vorticity (grey line) plotted as a function of depth at 90 km west and 250 km south (shown on other figures as a magenta line and point). Vorticity extrema coincide with well mixed regions and zeros with mixing barriers suggesting the density staircases are formed by the overturning cells.

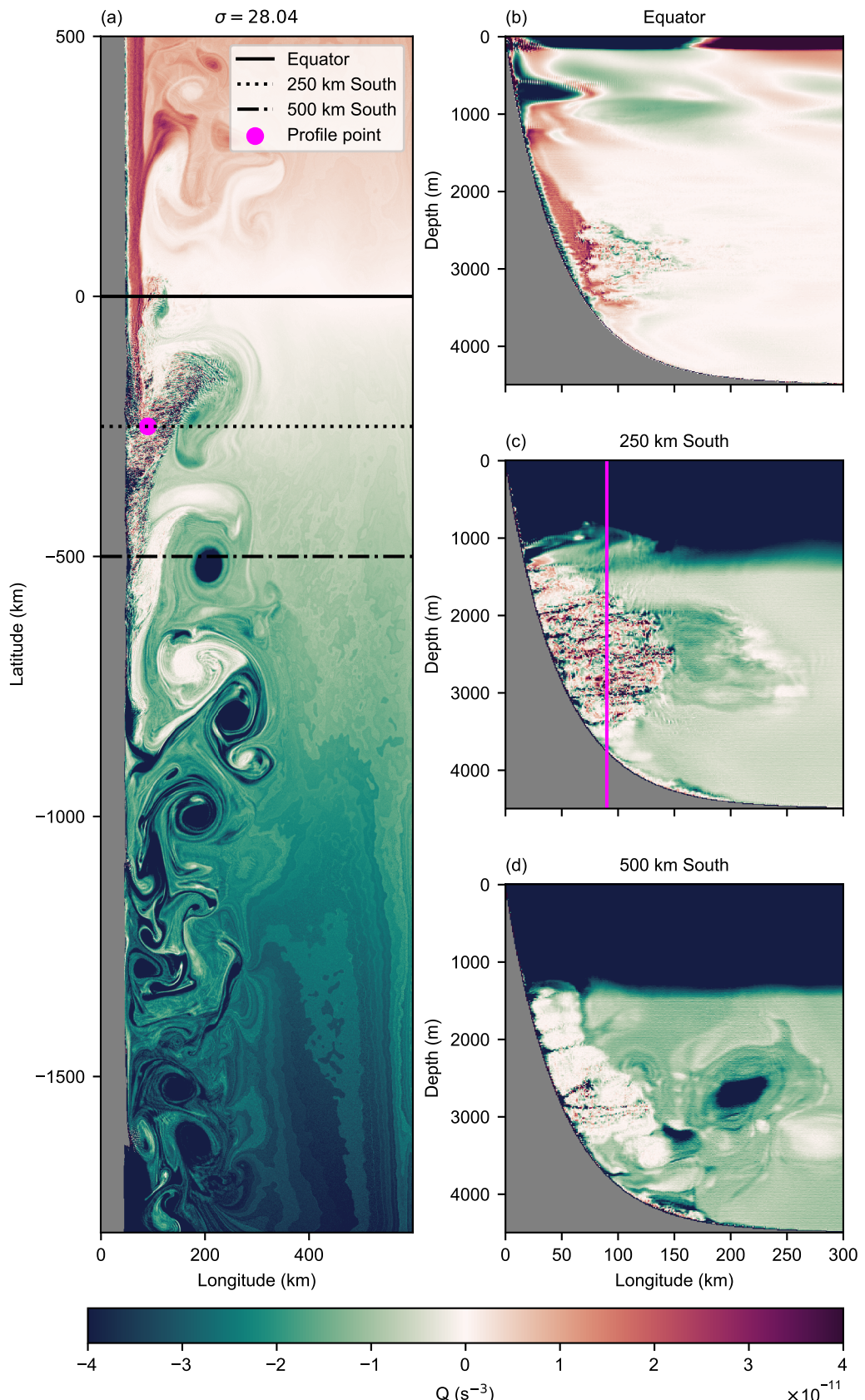


Figure 4.4: Potential vorticity after 23.6 days of model integration plotted on (a) the $\sigma = 28.04$ surface, (b) at the equator, (c) at 250 km south of the equator, and (d) at 500 km south of the equator. Black lines show the latitudes at which sections

4.5 Conclusions

Density staircases are step like features which become apparent when density is plotted as a function of depth and are common throughout the Earth's oceans. In an idealised model of a deep western boundary current crossing the equator we see density staircases form. The staircases are generated by overturning cells which are in turn generated by the excitement of symmetric instability as the current crosses the equator. Symmetric instability in cross-equatorial flows is excited due to the advection of anomalous potential vorticity from one hemisphere to another. The stacked overturning cells that generate the staircases are, however, a feature of symmetric instability regardless of what is forcing its excitement, suggesting we may see staircase formation in other symmetrically unstable flows — including when anomalous potential vorticity is induced by frictional torques or diabatic processes.

It is thought that diapycnal mixing may play an important role in closing the overturning budget of the Atlantic Meridional Overturning Circulation's deep limb. The amount of diapycnal mixing induced by symmetric instability in the deep western boundary current should be investigated further to ascertain whether the process may help to close the overturning budget.

Chapter 5

Ekman driven symmetric instability in a high latitude western boundary current

Brrrrrrr — Fraser Goldsworth

Bibliography

- Balmforth, N. J., Llewellyn Smith, S. G. and Young, W. R. (1998), ‘Dynamics of interfaces and layers in a stratified turbulent fluid’, *Journal of Fluid Mechanics* **355**, 329–358. doi: 10.1017/S0022112097007970.
- Bower, A., Lozier, S., Biastoch, A., Drouin, K., Foukal, N., Furey, H., Lankhorst, M., Rühs, S. and Zou, S. (2019), ‘Lagrangian Views of the Pathways of the Atlantic Meridional Overturning Circulation’, *Journal of Geophysical Research: Oceans* **124**(8), 5313–5335. doi: 10.1029/2019JC015014.
- Buckingham, C. E., Gula, J. and Carton, X. (2021), ‘The Role of Curvature in Modifying Frontal Instabilities. Part I: Review of Theory and Presentation of a Nondimensional Instability Criterion’, *Journal of Physical Oceanography* **51**(2), 299–315. doi: 10.1175/JPO-D-19-0265.1.
- Forryan, A., Naveira Garabato, A. C., Vic, C., Nurser, A. J. and Hearn, A. R. (2021), ‘Galápagos upwelling driven by localized wind–front interactions’, *Scientific Reports* **11**(1), 1–12. doi: 10.1038/s41598-020-80609-2.
- Griffiths, S. D. (2003), ‘The nonlinear evolution of zonally symmetric equatorial inertial instability’, *Journal of Fluid Mechanics* **474**(474), 245–273. doi: 10.1017/S0022112002002586.
- Haine, T. W. N. and Marshall, J. (1998), ‘Gravitational, Symmetric, and Baro-

clinic Instability of the Ocean Mixed Layer', *Journal of Physical Oceanography* **28**(4), 634–658. doi: 10.1175/1520-0485(1998)028<0634:gsabio>2.0.co;2.

Hoskins, B. J. (1974), 'The role of potential vorticity in symmetric stability and instability', *Quarterly Journal of the Royal Meteorological Society* **100**(425), 480–482. doi: 10.1002/qj.49710042520.

Hua, B. L., Moore, D. W. and Le Gentil, S. (1997), 'Inertial nonlinear equilibration of equatorial flows', *Journal of Fluid Mechanics* **331**, 345–371. doi: 10.1017/S0022112096004016.

Jackson, L. C., Kahana, R., Graham, T., Ringer, M. A., Woollings, T., Mecking, J. V. and Wood, R. A. (2015), 'Global and European climate impacts of a slowdown of the AMOC in a high resolution GCM', *Climate Dynamics* **45**(11–12), 3299–3316. doi: 10.1007/s00382-015-2540-2.

Jakoboski, J. K. (2019), Equatorial Ocean Dynamics Impacting Upwelling West of the Galápagos Archipelago, PhD thesis, MIT & WHOI.

URL: <https://hdl.handle.net/1721.1/123737>

Johannessen, O. M. and Lee, O. S. (1974), 'A deep stepped thermo-haline structure in the Mediterranean', *Deep-Sea Research and Oceanographic Abstracts* **21**(8), 629–639. doi: 10.1016/0011-7471(74)90047-3.

Kloosterziel, R. C., Carnevale, G. F. and Orlandi, P. (2017), 'Equatorial inertial instability with full Coriolis force', *Journal of Fluid Mechanics* **825**, 69–108. doi: 10.1017/jfm.2017.377.

Lambert, R. B. and Sturges, W. (1977), 'A thermohaline staircase and vertical mixing in the thermocline', *Deep Sea Research* **24**(3), 211–222. doi: 10.1016/S0146-6291(77)80001-5.

Marshall, D. P. and Pillar, H. R. (2011), ‘Momentum balance of the Wind-Driven and Meridional Overturning Circulation’, *J.Phys.Oceanogr.* **41**, 960–978. doi: 10.1175/201.

Melling, H., Lake, R., Topham, D. and Fissel, D. (1984), ‘Oceanic thermal structure in the western Canadian Arctic’, *Continental Shelf Research* **3**(3), 233–258. doi: 10.1016/0278-4343(84)90010-4.

Merryfield, W. J. (2000), ‘Origin of Thermohaline Staircases’, *Journal of Physical Oceanography* **30**(5), 1046–1068. doi: 10.1175/1520-0485(2000)030<1046:OOTS>2.0.CO;2.

Morel, Y., Gula, J. and Ponte, A. (2019), ‘Potential vorticity diagnostics based on balances between volume integral and boundary conditions’, *Ocean Modelling* **138**(April), 23–35. doi: 10.1016/j.ocemod.2019.04.004.

Ooyama, K. (1966), ‘On the Stability of the Baroclinic Circular Vortex: A Sufficient Criterion for Instability’, *Journal of the Atmospheric Sciences* **23**(1), 43–53. doi: 10.1175/1520-0469(1966)023<0043:OTSOTB>2.0.CO;2.

Plougonven, R. and Zeitlin, V. (2009), ‘Nonlinear development of inertial instability in a barotropic shear’, *Physics of Fluids* **21**(10). doi: 10.1063/1.3242283.

Ribstein, B., Zeitlin, V. and Tissier, A. S. (2014), ‘Barotropic, baroclinic, and inertial instabilities of the easterly Gaussian jet on the equatorial β -plane in rotating shallow water model’, *Physics of Fluids* **26**(5). doi: 10.1063/1.4875030.

Salmon, R. (1998), Hamiltonian Fluid Dynamics, in ‘Lectures on Geophysical Fluid Dynamics’, Oxford University Press, Oxford, pp. 295–378. doi: 10.1016/B0-12-512666-2/00246-7.

Schmitt, R. W., Ledwell, J. R., Montgomery, E. T., Polzin, K. L. and Toole, J. M. (2005), ‘Ocean science: Enhanced diapycnal mixing by salt fingers in the thermocline of the tropical atlantic’, *Science* **308**(5722), 685–688. doi: 10.1126/science.1108678.

Schmitt, R. W., Perkins, H., Boyd, J. D. and Stalcup, M. C. (1987), ‘C-SALT: An investigation of the thermohaline staircase in the western tropical North Atlantic’, *Deep Sea Research Part A, Oceanographic Research Papers* **34**(10), 1655–1665. doi: 10.1016/0198-0149(87)90014-8.

Schott, F. A., Dengler, M., Zantopp, R., Stramma, L., Fischer, J. and Brandt, P. (2005), ‘The shallow and deep western boundary circulation of the South Atlantic at 5°-11°S’, *Journal of Physical Oceanography* **35**(11), 2031–2053. doi: 10.1175/JPO2813.1.

Stern, M. E. (1960), ‘The “Salt-Fountain” and Thermohaline Convection’, *Tellus* **12**(2), 172–175. doi: 10.3402/tellusa.v12i2.9378.

Stone, P. H. (1966), ‘On Non-Geostrophic Baroclinic Stability’, *Journal of the Atmospheric Sciences* **23**(4), 390–400. doi: 10.1175/1520-0469(1966)023<0390:ONGBS>2.0.CO;2.

Tait, R. and Howe, M. (1968), ‘Some observations of thermo-haline stratification in the deep ocean’, *Deep Sea Research and Oceanographic Abstracts* **15**(3), 275–280. doi: 10.1016/0011-7471(68)90005-3.

Thomas, L. N., Taylor, J. R., Ferrari, R. and Joyce, T. M. (2013), ‘Symmetric instability in the Gulf Stream’, *Deep-Sea Research Part II: Topical Studies in Oceanography* **91**, 96–110. doi: 10.1016/j.dsr2.2013.02.025.

Xu, Q. and Clark, J. H. E. (1985), ‘The Nature of Symmetric Instability and Its Sim-

ilarity to Convective and Inertial Instability', *Journal of the Atmospheric Sciences* **42**(24), 2880–2883. doi: 10.1175/1520-0469(1985)042<2880:TNOSIA>2.0.CO;2.

Zeitlin, V. (2018), ‘Letter: Symmetric instability drastically changes upon inclusion of the full Coriolis force’, *Physics of Fluids* **30**(6), 061701–1 – 4. doi: 10.1063/1.5031099.

Zhou, H., Dewar, W., Yang, W., Liu, H., Chen, X., Li, R., Liu, C. and Gopalakrishnan, G. (2022), ‘Observations and modeling of symmetric instability in the ocean interior in the Northwestern Equatorial Pacific’, *Communications Earth & Environment* **3**(1). doi: 10.1038/s43247-022-00362-4.